frontiers | Frontiers in Soft Matter

TYPE Original Research
PUBLISHED 18 December 2023
DOI 10.3389/frsfm.2023.1329058

OPEN ACCESS

EDITED BY
Mohd Sajid Ali,
King Saud University, Saudi Arabia

REVIEWED BY
Animesh Pan,
University of Rhode Island, United States
Ajaya Bhattarai,
Tribhuvan University, Nepal

*CORRESPONDENCE
Erica Pensini,
epensini@uoguelph.ca

RECEIVED 27 October 2023
ACCEPTED 29 November 2023
PUBLISHED 18 December 2023

CITATION
Bartokova B, Marangoni AG, Laredo T and Pensini E (2023), Effect of sorbitan ester structure on the separation between tetrahydrofuran and water.
Front. Soft Matter 3:1329058.
doi: 10.3389/frsfm.2023.1329058

Effect of sorbitan ester structure on the separation between tetrahydrofuran and water

Bibiana Bartokova[1], Alejandro G. Marangoni[2,3], Thamara Laredo[4] and Erica Pensini[1,3]*

[1]School of Engineering, University of Guelph, Guelph, ON, Canada, [2]Food Science Department, University of Guelph, Guelph, ON, Canada, [3]Biophysics Interdepartmental Group (BIG), University of Guelph, Guelph, ON, Canada, [4]Chemistry Department, Lakehead University, Orillia, ON, Canada

This study separates tetrahydrofuran (THF)-water mixtures containing varying THF percentages, using sorbitan esters (Spans) with different tail characteristics. We probe the separation mechanisms using attenuated total reflectance-Fourier transform infrared spectroscopy and small angle X ray scattering (SAXS). THF and water are miscible and interact through hydrogen bonds. Water splits the COC absorbance band of THF into a peak at ≈1,070 cm^{-1} (crystalline THF) and a dominant peak at ≈1,050 cm^{-1} (glassy THF), indicating disorder. Depending on the Span, separation occurs for mixtures containing up to 70% THF (v/v, relative to water). Spans with unsaturated tails separate the lowest THF percentages. Tail length and number of Span tails enhances ordering of THF, and the crystalline THF peak at ≈1,070 cm^{-1} dominates. Spans interact with THF through hydrogen bonds, as reflected in the splitting of the COC band of THF. Furthermore, C-H...O hydrogen bonds cause a blueshift in the $\nu_{as}(CH_2)$ band of Spans with increasing THF. This effect is most significant in Span 40 and 60, indicating that they interact with THF more strongly than Span 20, Span 80 and Span 85. In contrast, they interact with water less strongly than Span 20, Span 80 and Span 85, as indicated by their flocculation at low THF percentages. Therefore, we propose that separation between THF and water occurs *primarily* through two mechanisms: 1) Span 20, Span 80 and Span 85 compete against THF for interactions with water through their hydrophilic head, and 2) Span 40 and Span 60 preferentially interact with THF through their tails. Nonetheless, water also interacts with the heads of Span 40 and Span 60, as indicated by SAXS. SAXS shows that in THF Spans self-assemble into micelles, which aggregate into either surface fractals or mass fractals. There are two persistence lengths because of the limited order in THF. Water orders self-assembled structures, likely by favoring the formation of micelles which host water in their interior. Therefore, we identify a single persistence length (≈25 Å), representative of the distance between the micelle centers.

KEYWORDS

mixing behaviour, separation, sorbitan esters, hydrogen bonding, solvent structure

1 Introduction

THF, acetonitrile, dimethylformamide or methanol are water miscible pollutants used in industrial processes (Sales et al., 2013; Yin et al., 2017; Earnden et al., 2022a; Earnden et al., 2022b; Earnden et al., 2022c; Marshall et al., 2022; Bartokova et al., 2023a). They are found in industrial wastewater as well as in groundwater, in the case of spills such as those caused by

the notable Ohio trail derailment accident (2023). Our study focuses on THF, which is used as a stabilizer for chlorinated solvents, as well as to produce pharmaceuticals and pesticides (Sales et al., 2013; Yin et al., 2017).

Beyond their intrinsic toxicity, spills of water miscible solvents are particularly problematic because they can rapidly migrate in impacted aquifers, harming downstream receptors (Bartokova et al., 2023a). Furthermore, their separation from water presents greater challenges compared to water-immiscible pollutants, such as hydrocarbons (Bartokova et al., 2023a). These can be removed from water through mechanical separation methods (e.g., coalescers (Kolehmainen and Turunen, 2007)) or chemical methods (such as oxidation (Wang et al., 2013; Malakahmad and Ho, 2017; Besha et al., 2018)). Also, when they are present in groundwater below levels at which they are toxic to the bacteria, they can biodegraded (Boonchan et al., 1998; Belhaj et al., 2002; Barman et al., 2017). Since biodegradation tends to be a fairly slow process, there are limitations to its use in the case of rapidly migrating pollutants. These consideration also apply to phytoremediation using plants (Hall et al., 2011; Sun et al., 2011). Moreover, phytoremediation is only effective for shallower contamination, which can be reached by the roots of the plants. In the case of miscible organic solvents, pervaporation is often used (Yoshikawa et al., 2002). Beyond its high energy cost, its implementation for the treatment of impacted aquifers is not feasible. This is because complex treatment units could be integrated in a chemical plant, but they cannot be built as part of a remediation plant on polluted sites. Therefore, it is necessary to identify cost-effective, facile methods to separate miscible solvents from either industrial wastewater or groundwater. These methods were scant until our most recent research.

Previous studies used CO_2 switchable species (Jessop and Cunningham) or increased the hydrophobicity of the organic solvent (Longeras et al., 2020) to increase their incompatibility with water, thereby leading to separation. Other studies used species that preferentially interact with water, at the expense of its interactions with the solvent. Examples of these species are sugars and their alcohols (Wang et al., 2008; Dhamole et al., 2010; de Brito Cardoso et al., 2014) as well as salts, such as sodium chloride and choline salts) (Tabata et al., 1994; Souza et al., 2015).

In our recent research, we have used amphiphiles to separate miscible solvents from water. Examples include sodium lauroyl lactylate (Marshall et al., 2022), glycerol monooleate (Earnden et al., 2022c), fatty acids (Earnden et al., 2022a; Earnden et al., 2022b; Bartokova et al., 2023a) and a sorbitan ester (Span 80, (Bartokova et al., 2023b),). In these studies, we showed that separation involves preferential interactions either between water and the amphiphile [e.g., in the case of Span 80, (Bartokova et al., 2023b)] or preferential interactions between the solvent and the amphiphile [e.g., in the case of stearic acid, (Bartokova et al., 2023a)]. To investigate interactions between water and other components in the mixture (solvent and amphiphiles), we probed the OH stretch band of water using Attenuated Total Reflectance–Fourier Transform Infrared (ATR-FTIR) spectroscopy. We deconvolved the OH stretch peak into four peaks, representing water species with different coordination to other molecules in the mixtures. Specifically, we considered double (DD) and single (SD) hydrogen (H) bond donors, and double (DA) and single (SA) H bond acceptors. Based on this analysis, we concluded that separation is promoted when amphiphiles interact with water the same way the solvent does, i.e., when amphiphiles compete with the solvent for interactions with the same water species. We also analyzed H bonding of solvent with hydrophobic amphiphiles, such as stearic acid (Bartokova et al., 2023a). We showed that the COC band of THF contains information about H bonding, by comparing changes of the OH stretch band of water and the COC band of THF, in THF-water mixtures (Bartokova et al., 2023a). By analyzing this band, we demonstrated that stearic acid separates water from THF because it competes for interactions with the same THF species, i.e., THF molecules that H bond and coordinate the same way with other molecules in solution (Bartokova et al., 2023a).

Furthermore, we highlighted that the tail plays an important role in separation. For example, separation between THF and water does not occur upon adding acetic acid, although the structure of acetic acid is the same as the head of stearic acid (Bartokova et al., 2023a). Given this similarity, both acetic acid and stearic acid H bond with THF the same way (Bartokova et al., 2023a). We proposed that the tail of stearic acid promotes H bonding between THF and the hydrophilic tail at the expense of THF-water interactions. In contrast, in the absence of the tail, acetic acid can H bond either water or THF, thereby enabling the existence of a ternary solution. Indeed, solubility plays a key role. Specifically, separation is favored when the amphiphile added has intermediate solubility in the mixture, and is soluble in either water or the solvent, but not both (Marshall et al., 2022). In ternary mixtures where all components are miscible two by two, there are instances where separation may still occur, but predictions of the mixing behaviour are notably more complex (Bartokova et al., 2023c). Solubility of the amphiphile in each component and in the mixture is clearly affected by the tail. While our previous studies started highlighting the role of the tail, we had not yet conducted a systematic analysis of the role of the tail on solvent separation. The current study aims to fill this research gap.

In particular, the objective of this study is to expand on our previous research, comparing the separation between THF and water using sorbitan esters with a different tail structure (e.g., tail length and hence hydrophobicity, and double vs. single bonds in the tail). Specifically, we investigate interactions (H bonding) between THF and different sorbitan esters, comparing them with interactions between THF and water. We also analyze the role of the tail on THF ordering and its separation from water.

This objective supports the overall goal of our research, which is to develop a robust approach to predict the separation of water from miscible solvents, and to identify the most effective amphiphiles for water purification. The toolbox we are building relies on calculated values for H bonds between solvent-water couples, amphiphile-water couples, as well as amphiphile-solvent couples. We are calculating these values in our research. Values estimated on representative amphiphile and solvents will be used to provide initial estimated for other similar compounds, predicting the mixing behaviour of ternary mixtures. Our toolbox also relies on building a systematic and quantitative understanding of the effect of the tail characteristics and amphiphile solubility. The current study will be followed by others, where broader groups of amphiphiles will

be used to consolidate the portion of our predictive toolbox focused on the tails. Our approach will be complementary to models such as COSMO, which we recently used to predict activity coefficients, because they are correlated to solvent separation (Bartokova et al., 2023a).

2 Materials and methods

2.1 Materials

Sorbitan esters (Span 20, Span 40, Span 60, Span 65, Span 80 and Span 85) were purchased from Sigma Aldrich (Canada). Their structure and hydrophilic lipophilic balance (HLB) number are given in Table 1 and Scheme 1. THF (reagent grade, Caledon laboratory chemicals) was purchased from Fisher Scientific (Canada). All experiments were conducted using deionised (DI) water.

2.2 Bottle tests

Samples were prepared using 40 g/L of sorbitan esters and mixtures containing varying percentages of DI water and THF (0%–100% THF, v/v relative to water). Samples were agitated by hand for 10 s after heating to 65°C for 2 min, using a hotplate. Samples were then cooled and observed at 20°C under quiescent conditions for 24 h, to qualitatively determine their phase behavior. These same samples were also imaged using optical microscopy (Section 2.3) and analyzed using ATR-FTIR (Section 2.4).

2.3 Optical microscopy

A VHX-5000 digital microscope (Keyence) was used to image THF-water emulsions stabilized with different sorbitan esters.

2.4 Attenuated total reflectance–Fourier transform infrared spectroscopy (ATR-FTIR)

Absorbance spectra were collected using an ATR-FTIR spectrometer (Thermoscientific Nicolet Summit FTIR spectrometer with an Everest ATR), with an accompanying IR solution software (Omnic 9, Thermo Fisher Scientific). Each spectrum was the average of 10 scans, with a resolution of 2 cm^{-1}. The wavenumbers ranged from 400 cm^{-1} to 4,000 cm^{-1}. Measurements were conducted at least in duplicate.

Spectra were analyzed using Quasar 1.5.0 (Orange-Spectroscopy software), using a rubber band baseline correction. Additionally, the spectra where normalized using min-max normalization. To this end, each spectrum was divided by its Abs_{max}–Abs_{min} range.

2.5 Synchrotron based small angle X-ray scattering (SAXS)

SAXS experiments were carried out at the Canadian Light Source Synchrotron (CLS) on the Brockhouse Diffraction Sector Undulator Beamline (BXDS-IVU) (Leontowich et al., 2021), to identify the self-assembly of sorbitan esters into either pure THF or THF-water mixtures containing 2% water (relative to THF). In this study, samples were introduced into quartz tubing (Polyamide 0.0575″ ID x 0.0615″ OD), which was sealed to avoid solvent evaporation during data collection. A clay compound was used for sealing. SAXS data was collected with a Rayonix MX300HE detector (8,192 × 8,192 pixels) with 2 × 2 binning (4,096 × 4,096 pixel) for an effective pixel size of 73.242 μm with background stability mode ON. SAXS patterns were collected with a photon energy of 12.18 keV and sample-to-detector distance of ~233 cm. SAXS patterns were collected in transmission geometry with a 120 s dwell time. Patterns were processed with GSASII (Argonne National Laboratory (C), 2010). This product includes software developed by the UChicago Argonne, LLC) (Toby and Von Dreele, 2013; Von Dreele, 2014). SAXS data was calibrated with silver behenate (AgBeh) and instrument parameters such as sample-to-detector distances, detector tilt, beam centre, were refined as described elsewhere (Von Dreele, 2014). SAXS patterns were integrated from q = 0.012 to q = 0.637 $Å^{-1}$. Measurements were done in duplicate for each sample.

Absolute intensity with background removed as a function of the scattering vector, q, were fitted to a model recently developed by our group. It has the general form,

$$I(q) = Cq^{-s} + I_0 \exp^{-0.5\left(\frac{q}{\sigma_0}\right)^2} + \sum_{i=1}^{n} I_i \exp^{-0.5\left(\frac{q-q_{p,i}}{\sigma_{p,i}}\right)^2} \quad (1)$$

The scattering intensity is interpreted as arising from scale-independent fractal scattering in the low q-range, superimposed on top Guinier's form factor, namely a zero-mean Gaussian. Any periodicities arising from other correlations in the system are captured by non-zero mean Gaussians. In our case, we only required one zero mean Gaussian and one non-zero mean Gaussian.

The fractal dimension is captured in the modeling process by writing the scattering intensity, such as

$$I(q) \sim q^{D_s - 2\left(D_m + D_p\right) + 2d} \quad (2)$$

This is a simple power-law decay on a double logarithmic scale within a given q-range limited by reciprocal fractal outer and inner cutoffs, q_{oc} and q_{ic}, respectively, i.e., when $q_{oc} < q < q_{ic}$. It is also known in the literature as the fractal region. Here, q is the module of the scattering vector, D_s, D_m and D_p are the surface, mass and respectively the pore fractal dimensions, and d is the Euclidean dimension of the space in which the fractal is embedded. In the case of surface fractals $d-1 < D_s < d$, $D_m = D_p = d$ and the scattering intensity reduces to $I(q) \sim q^{Ds-2d}$. For mass fractals $0 < D_m < d$, $D_m = D_s$ and $D_p = d$, and $I(q) \sim q^{-Dm}$, while for pore fractals $D_p = D_s$ and $D_m = d$, and thus $I(q) \sim q^{-Dp}$. Therefore, one can obtain the fractal dimension from the slope (s) of the experimental scattering curve. Moreover, one can differentiate between mass and surface fractals, i.e., if the measured slope is $s < d$ then the sample is a mass fractal, while if $d < s < d + 1$, the sample is a surface fractal. For a surface fractal, D_s is equal to 2 for a perfectly smooth surface, and approaches 3 for a highly folded/convoluted surface.

10.3389/frsfm.2023.1329058

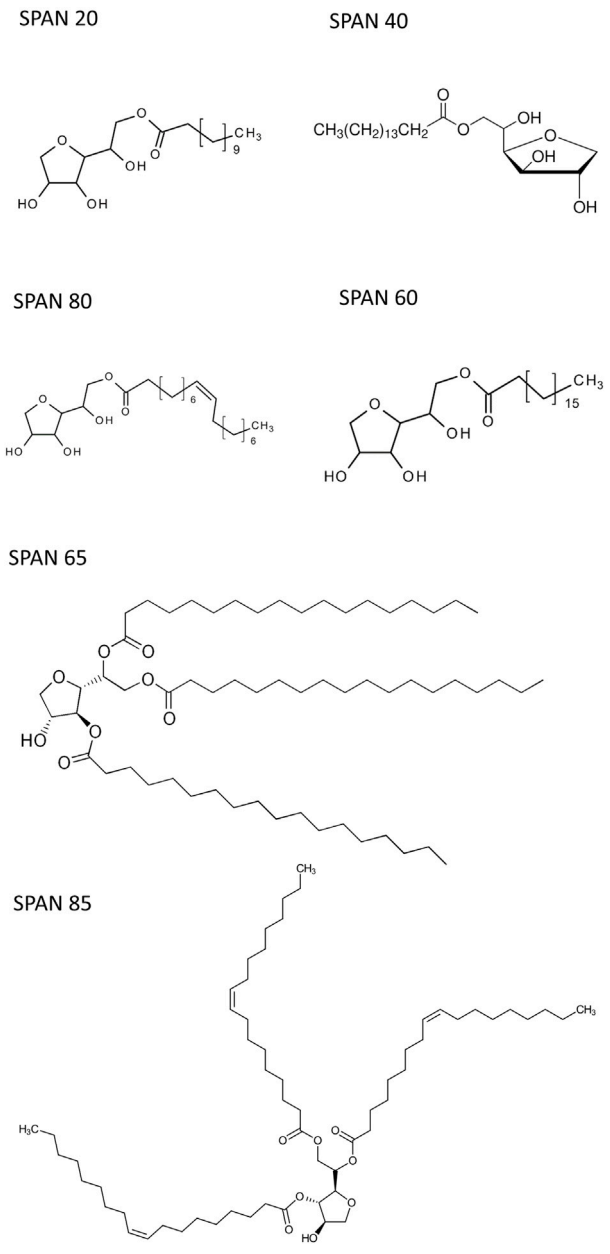

SCHEME 1
Structures of the compounds used.

TABLE 1 HLB number and tail length of the Spans used in this study.

Surfactant name	HLB	Tail length
Span 20 (sorbitan monolaurate)	8.6	11
Span 40 (sorbitan monopalmitate)	6.7	15
Span 60 (sorbitan monostearate)	4.7	17
Span 80 (sorbitan monooleate)	4.3	17
Span 65 (sorbitan tristearate)	2.1	17 on each tail, 3 tails
Span 85 (sorbitan trioleate)	1.8	17 on each tail, 3 tails

TABLE 2 Summary of the different phases observed in THF-water mixtures, with different THF to water ratios, and with different sorbitan esters. This table reflects observations with the naked eye and with an optical microscope, over a 24 h period. The colors of the cells distinguish different phase behaviours, and are used as visual aid. 1L = one liquid phase, based on observations with the naked eye and under an optical microscope; 1L + F = one liquid phase, based on observations with the naked eye and under an optical microscope, mixed with flocculated surfactant; E= emulsion, as seen under an optical microscope; 2L = separation into bulk phases, as seen with the naked eye in bottle tests.

Span	HLB	Tail			THF % (v/v, relative to water)								
		Number of carbons	Number of tails	Bonds	10	20	30	40 (L)	50 (L)	60 (L)	70 (L)	80 (L)	90 (L)
Span 20	8.6	11	1	Single	E	E	E	2	2	2	1	1	1
Span 40	6.7	15	1	Single	1L + F	1L + F	1L + F	2	2	2	2	1	1
Span 60	4.7	17	1	Single	1L + F	1L + F	1L + F	2	2	2	2	1	1
Span 80	4.3	17	1	Double	E	E	E	2	2	2	2	1	1
Span 65	2.1	17	3	Single	1L + F	E	E	2	2	2	2	2	1
Span 85	1.8	17	3	Double	E	E	E	2	2	2	2	2	1

The term q_p corresponds to the center of the Gaussian peak, while σ corresponds to the standard deviation of the Gaussian, which characterizes the width of the distribution.

The model was fitted to the data by non-linear regression using Prism 10.1 (GraphPad Software, San Diego, CA). We used a standard nonlinear regression routines (Levenberg, 1944; Marquardt, 1963), and data were weighted by $1/Y^2$. This was done to ensure that solutions were stable and in order to determine confidence intervals.

The center position of the Gaussian peaks in reciprocal space was converted to its corresponding value in direct space, d_p, by $d_p = 2\pi/q_p$. To determine the domain size, correlation length, coherence length, sometimes referred to the persistence length of the scattering event related to the Gaussian peaks we used an approximation based on the standard Scherrer model:

$$\xi = \left(\frac{K2\pi}{\Delta q}\right) \tag{3}$$

The term Δq refers to the full width half maximum of a peak. The conversion of a standard deviation to a full-width half maximum is $FWHM = 2\sqrt{2\ln 2}\sigma$, while the shape factor is usually assumed to be K = $K = 2\sqrt{\frac{\ln 2}{\pi}}$ for spherical domains of cubic symmetry. The correlation length can then be calculated from the standard deviation of the Gaussian using:

$$\xi = \left(\frac{\sqrt{2\pi}}{\sigma}\right) \tag{4}$$

2.6 FTIR spectromicroscopy

FTIR spectromicroscopy (in ATR mode) was used to analyze emulsions prepared using different sorbitan esters and varying percentages of THF and water.

Measurements were conducted at the Canadian Light Source (CLS) in Saskatoon (Canada) using an Agilent Cary 670 FTIR Interferometer with Cary 620 Microscope, employing a 2D Focal Plane Array MCT-A detector. The hyperspectra were collected in transmission mode by placing 0.5 µL in between two calcium fluoride windows separated by a 10 µm Teflon spacer. This technique was used to map the samples, characterizing compositional differences between the interior and the exterior of emulsified droplets.

3 Results and discussion

THF and water are freely miscible in one another in binary solutions. Our previous study revealed that Span 80, a sorbitan ester, separates THF from water (Bartokova et al., 2023b). Here, we examine THF-water separation with different sorbitan esters (cf. Table 1), to assess the effect of their structure, and their tail in particular, on the mechanisms of solvent-water separation.

Note that in our study, separation was qualitatively assessed through bottle tests, optical microscopy and FTIR spectromicroscopy (Table 2). Our previous research conducted using Span 80 quantitatively showed that this sorbitan ester increases the water purity, but does not reduce THF to values compatible with legislative limits. These are for instance 50–1,300 µg/L in different states in the United States (Isaacson et al., 2006). Span 80 is also one of the sorbitan esters analyzed in our current study. A modeling study reports that swing distillation could theoretically achieve up to 99.9% removal of THF from water (Lee et al., 2011). Swing distillation is, however, energy intensive. Another study conducted using electrooxidation reports that THF removal was higher than 90% with suitable electrodes (Urtiaga et al., 2014). However, electrokinetic methods also use energy and require the installation of electrodes in impacted aquifers, which can be challenging and costly. The goal of our study is to reduce the concentrations of THF in water using low energy approaches, to then allow for subsequent treatments to be effective. As an example, a study reported the successful removal of THF from water using anaerobic bacteria and membranes (Hu et al., 2018).

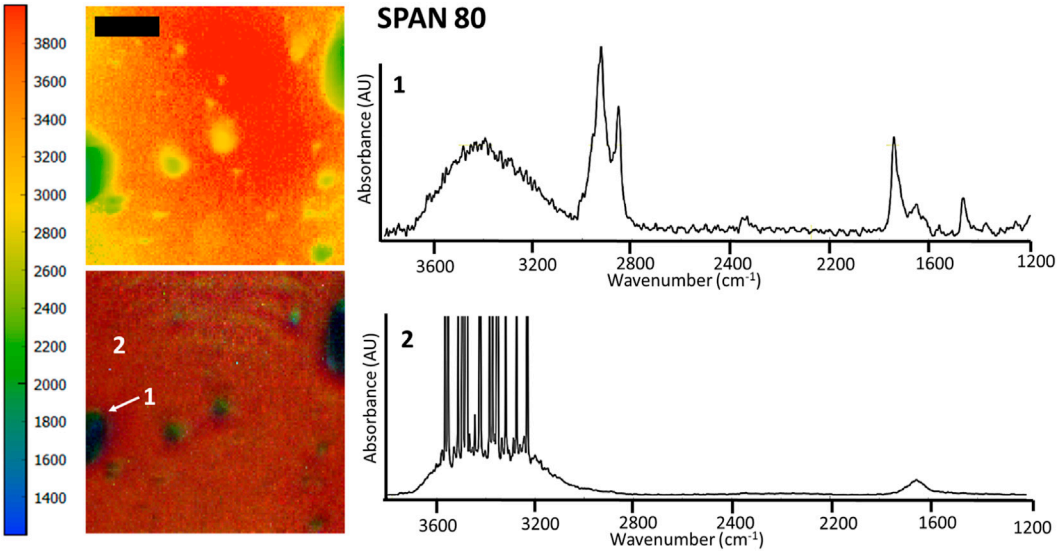

FIGURE 1
FTIR spectromicroscopy images of THF-rich droplets in water, stabilized by 40 g/L Span 80. Samples contained 30% THF (v/v, relative to water). The scale bar is 100 µm. The colored scale bar shows the wavenumbers, providing an indication of the different chemical composition of droplets and the bulk phase in the rainbow colored image (red/orange = water, labelled as 2, with a dominant OH stretch at 2,500–4,000 cm^{-1}; green = THF and sorbitan esters, labelled as 1). Note that in these experiments samples were inserted in a compression cell, explaining the distortion in the droplet shape and their relatively large size. The compression cell was used to limit the thickness of the water layer. Nonetheless, the OH stretch band of water is saturated in the IR spectra of the water-rich phase (spectrum 2). FTIR spectromicroscopy images of THF-water mixtures separated by Span 60 and Span 85 are in the supporting information file (Supplementary Figure S1.2).

TABLE 3 D and fractal type of sorbitan ester self assembled structures, for different sorbitan esters.

	THF			
	D	Fractal type	Persistence length 1	Persistence length 2
Span 20	2.13	Surface	25.1	11.9
Span 40	2.78	Mass	25.5	13.7
Span 60	N/A			
Span 65	2.41	Mass	27.2	12.1
Span 80	2.38	Surface	26.6	15.9
Span 85	2.38	Surface	27.4	21.6
	THF +2% water			
	D	Fractal type	Persistence length 1	Persistence length 2
Span 20	2.75	Surface	27.4	19.3
Span 40	2.18	Surface	27.2	24.3
Span 40, replicate	2.21	Surface	27.3	23.9
Span 60	2.46	Surface	26.9	23.3
Span 65	2.27	Surface	23.9	23.2
Span 80	2.72	Surface	23.2	24.8
Span 85	2.15	Mass	24.5	31.6
Span 85, replicate	2.17	Mass	24.4	32.1

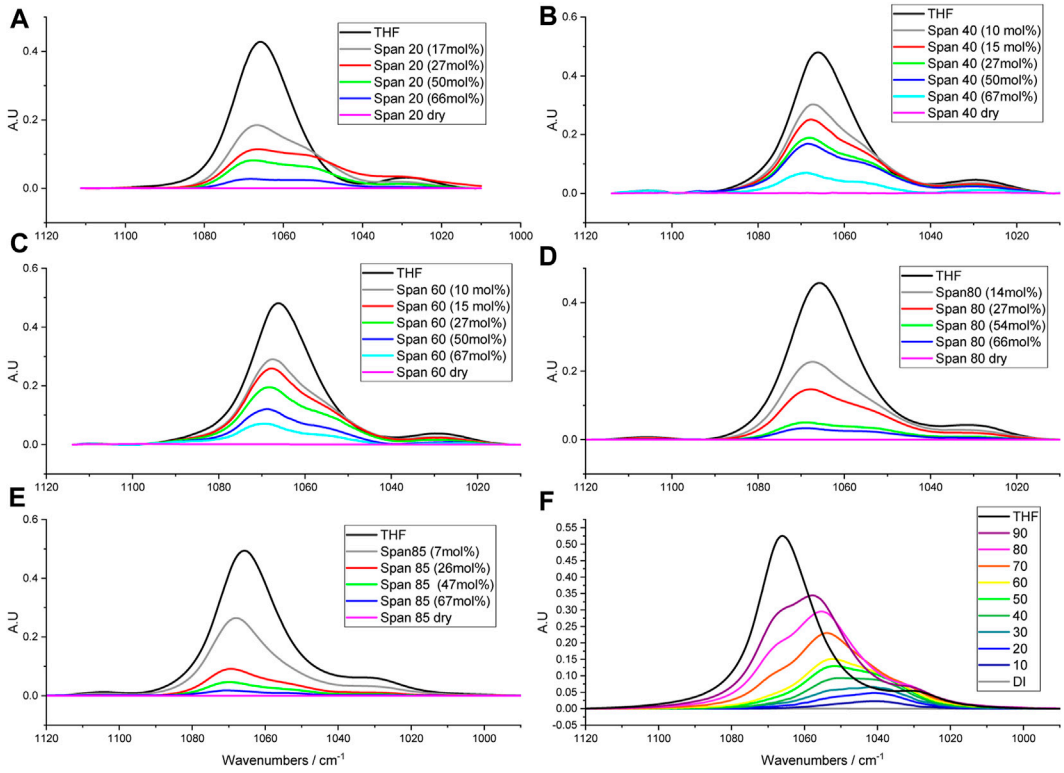

FIGURE 2
Absorbance spectra in the COC region for THF mixtures with different sorbitan esters. **(F)** was reprinted from Bartokova et al. (2023a) with permission. **(A–E)** show the spectra for THF mixtures with different Spans. **(F)** shows THF mixtures in water, containing different THF percentages. In **(F)**, deionised water is abbreviated as DI.

Bacterial remdiation is energy effective, but bacteria can remediate pollutants only below concentrations at which they are toxic to them. Therefore, our approach can represent the first step in a treatment train for the removal of THF from water. Identifying the mechanism of separation and the surfactant characteristics that lead to effective separation will allow us to optimize this first step.

Bottle tests and optical microscopy show that separation occurs at THF to water ratios dependent on the type of sorbitan ester (cf. Table 2; Figure 1; Supplementary Figures S1.1–S1.3). Specifically, we observe that both the hydrophobic lipophilic balance (HLB) number and saturation of the tail affect the THF to water ratio at which separation occurs.

While all sorbitan esters are hydrophobic (soluble in THF, insoluble in water), Span 20 has the highest HLB number (HLB = 8.6). It yields emulsions with 10%–30% THF (v/v, relative to water), free layers with 40%–60% THF and one liquid phase with 70%–80% THF. Span 40 (HLB = 6.7), Span 60 (HLB = 4.7) and Span 80 (HLB = 4.3) have intermediate HLB numbers. They separate THF from water into free layers with THF percentages ranging from 40% to 70%, while yielding one liquid phase only at 80% THF. With Span 40 and Span 60, separation does not occur with 30% THF or less, where the observed turbidity is due to flocs (Supplementary Figure S1.2). With Span 80, emulsions are observed at 30% THF or below (Supplementary Figure S1.2). Although Span 80 and Span 60 have similar HLB and the same tail length, Span 80 differs from Span 60 in that it has a double bond in its tail (i.e., its tail is unsaturated). Finally, Span 65 (HLB = 2.1) and Span 85 (HLB = 1.8) have the lowest HLB number, and they yield free phases with THF percentages from 40% to 80% THF. With 20%–30% THF, they yield emulsions. Finally, with 10% THF and Span 65, the observed turbidity is due to flocs (Supplementary Figure S1.2), while emulsions form with Span 85. Note that, similar to Span 80 and Span 60, Span 65 and 85 have similar HLB and the same tail length for each of their three tails. However, Span 85 has double bonds in its tails, while Span 65 does not. In both cases, double bonds in the tail (i.e., unsaturated tails) promote separation at the lowest THF percentages.

In our previous study, we explained water-THF separation by Span 80 based on the ability of Span 80 to compete against THF for hydrogen (H) bonding with water (Bartokova et al., 2023b). Here, we explore the alternative hypothesis that sorbitan esters interact with THF, competing against water. In our previous studies, we investigated H bonding between water and THF by probing the OH stretch band of water (Earnden et al., 2022b; Bartokova et al., 2023b). Water species coordinate differently with other molecules in solution. In particular, they can donate one (single donors, SD) or two (double donors, DD) hydrogens, and accept one (single acceptor, SA) or two (double acceptor, DA) hydrogens (Bartokova et al., 2023a; Bartokova et al., 2023b). Therefore, water species include the following: SD-DA (coordination = 3, at ~2,850–3,200 cm^{-1}), SD-SA (coordination = 2, at ~3,200–3,300 cm^{-1}), DD-SA (coordination = 3, at ~3,400–3,550 cm^{-1}) and DD-DA (coordination = 4, at

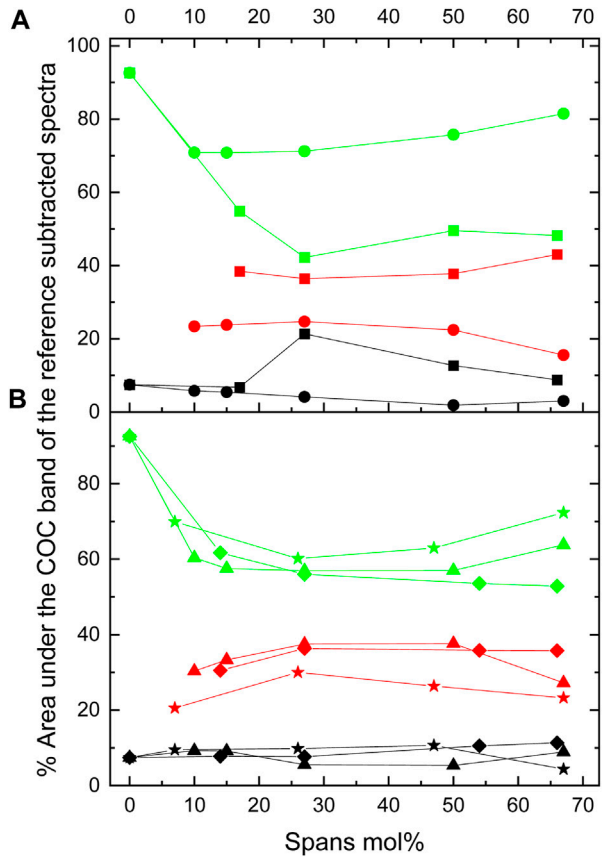

FIGURE 3
Percent areas under the COC band. These areas were obtained from the deconvolution of the dry reference subtracted COC band located at 1,030 (black), 1,055 (red), and 1,070 (green) cm^{-1} for **(A)** THF + Span 20 (squares) and THF + Span 60 (circles) and **(B)** THF + Span 40 (triangles), THF + Span 80 (diamonds) and THF + Span 85 (stars).

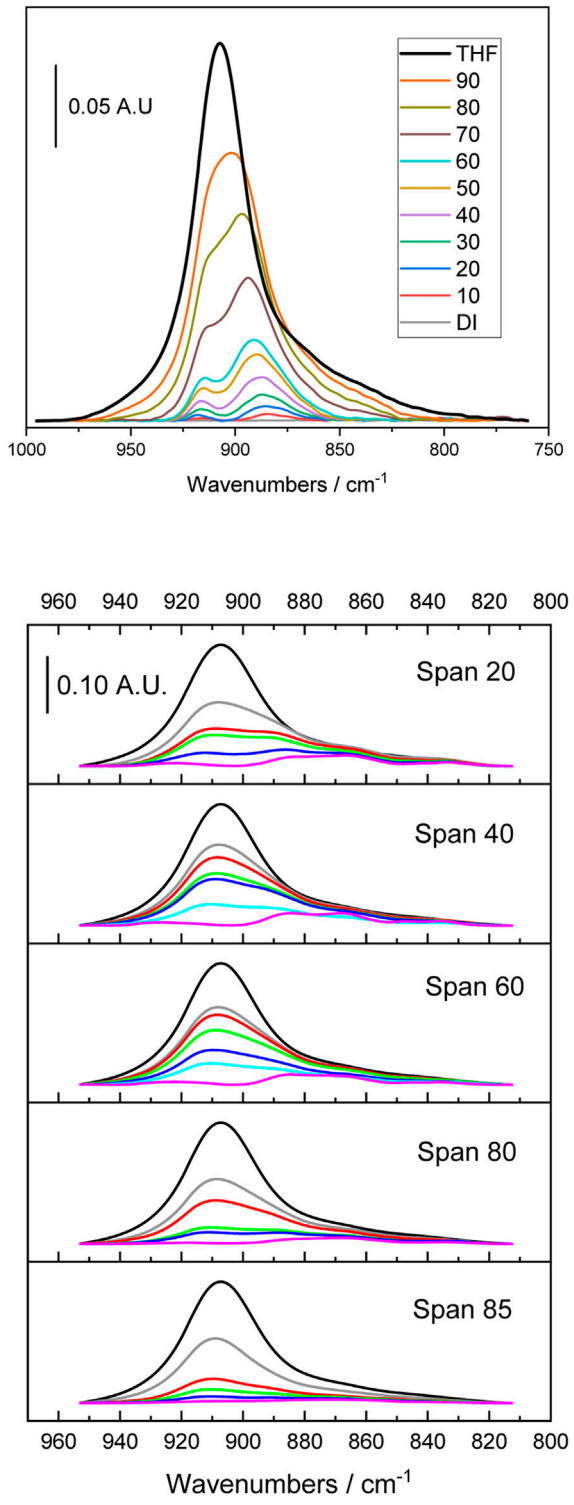

FIGURE 4
δ(C-C-O) band of THF upon mixing with water and with the different sorbitan esters. The colors match the concentrations indicated in Figure 2.

~3,300–3,400 cm^{-1}). In some instances, water species are intermediate between these four main species, as indicated by their peak position. The relative abundance of each water species can be estimated from the area of each of the peaks representing them. In our previous research, we found that in pure water SD-SA and DD-DA are the most abundant species, and have similar abundance (Bartokova et al., 2023a; Bartokova et al., 2023b). THF alters the distribution of water species, because it H bonds water and mainly accepts hydrogens (Patel et al., 2023). Therefore, DD-SA dominate at high THF percentages (above 70%) (Patel et al., 2023). Instead, DD-DA is dominant up to 40% THF. At intermediate THF percentages (50%–70% THF), the dominant water species is intermediate between DD-DA and SD-SA. The COC peak of THF at ≈1,065 cm^{-1} can also reveal H bonding between THF and water. Upon mixing with water, the COC peak of THF shifts and splits, as seen in Figure 2. Our recent study compared the OH stretch band of water and the COC band of THF, in THF-water mixtures (Bartokova et al., 2023a). This comparison showed that THF species that interact with DD-SA water species correspond to the 1,070 cm^{-1} peak in the COC band. The peak at 1,050 cm^{-1} dominates with >30% THF (v/v, relative to water), and it is related to THF species that mainly accept a single H. These water species correspond to SD-SA below 30% THF, and to species intermediate between SD-SA and DD-DA above 30% THF. Finally, the peak at 1,040 cm^{-1} corresponds to THF species that interact with SD-DA and DD-DA water species. In light

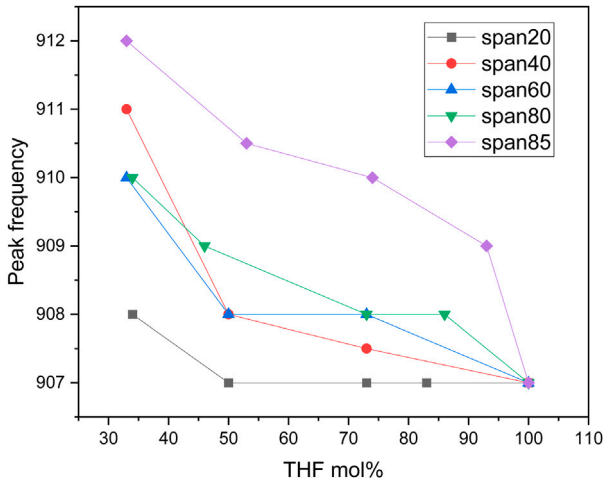

FIGURE 5
Center position of δ(C-C-O) peak upon mixing different mole percentages of THF with different sorbitan esters.

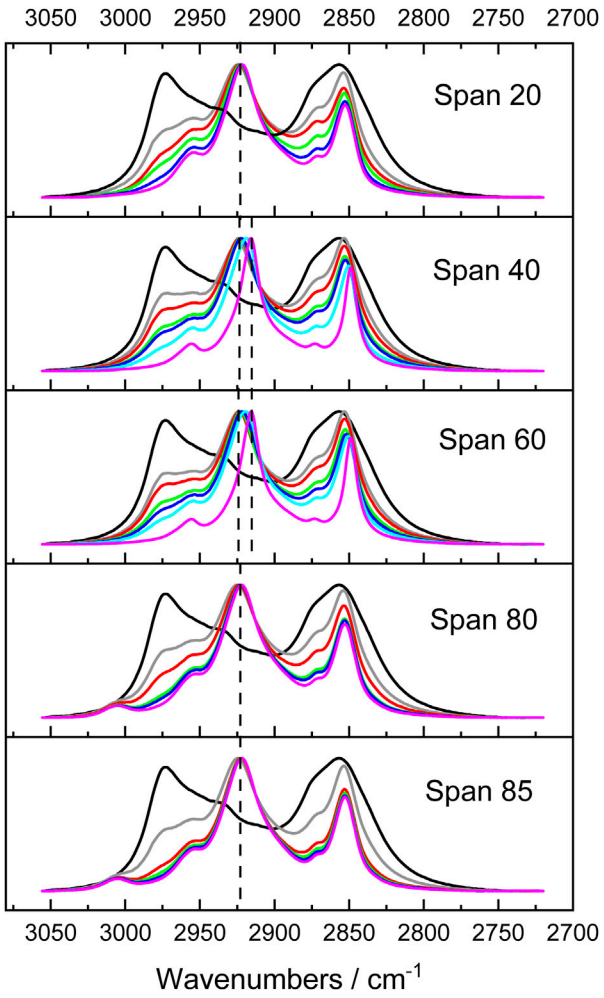

FIGURE 6
Comparison between the $\nu_{as}(CH_2)$ band of different sorbitan esters, with varying percentages of THF. Black: neat THF; grey: 66 mole% sorbitan ester; red: 50 mole% sorbitan ester; green: 27 mole % sorbitan ester; blue: 17 mole% sorbitan ester; pink: neat sorbitan esters.

of our previous study, we now use the COC band to study H bonding between THF and water, and between THF and sorbitan esters.

In particular, we analyze the COC band of THF to probe the hypothesis that sorbitan esters H bond THF. We also compare how H bonding of THF with water and with sorbitan esters affects the COC band of THF. With pure THF, we observe a dominant COC stretch peak at ≈1,070 cm^{-1} (Liu et al., 2022), and a significantly smaller peak at 1,027 cm^{-1} (Sionkowska and Płanecka, 2013) (Figure 1). As mentioned above, upon mixing with water, the peak at ≈1,070 cm^{-1} splits into three peaks, at ≈1,070 cm^{-1}, ≈1,050 cm^{-1} and ≈1,040 cm^{-1}. A previous study on THF hydrates reports that peaks associated with the CO stretch are affected by temperature, with a single CO stretch peak at 80 K (−193°C), a shoulder at 40 K (−233°C) and splitting at 13 K (−260°C) (Fleyfel and Devlin, 1991). Specifically, at 13 K the band at 1,070 cm^{-1} splits into 1,071 and 1,076 cm^{-1}. The authors attribute this band to crystalline THF and ascribe its split to the distribution of THF molecules over two unequal positions in the hexacaidecahedral water cages (Fleyfel and Devlin, 1991). In addition to the crystalline THF band at 1,070 cm^{-1}, the authors also identify a band at 1,052–1,054 cm^{-1} and ascribe it to less ordered (or glassy) THF. In our study, a peak at ≈1,050 cm^{-1} (glassy THF) appears upon mixing with water, while being absent for pure THF at ambient pressure and 20°C (Figure 2). Importantly, upon mixing with water, the peak at ≈1,050 cm^{-1} (glassy THF) is more prominent than the peak at 1,070 cm^{-1} (crystalline or ordered THF). This result is in agreement with a previous study, which also reports that mixing THF with water increases the proportion of amorphous (glassy) THF (Aliaga et al., 2011). Note that our results were obtained at ambient pressure. A split of the CO stretch band was also previously observed upon crystallizing methanol by super-pressing it to pressures of 101 kbar (Mammone et al., 1980).

Sorbitan esters also interact with THF through H bonds, as indicated by splitting of the COC band in THF-sorbitan ester mixtures. We propose that H bonding occurs between the oxygen on the ether ring of THF and the OH groups of the sorbitan esters. Qualitatively, we observe that this interaction results in a shift of the OH stretch band of sorbitan esters (Supplementary Figure S1.4). Figure 2 shows the COC band of THF, which can be deconvolved into three peaks at ≈1,050 cm^{-1} (glassy THF), at ≈1,070 cm^{-1} (crystalline THF) and at ≈1,030 cm^{-1}. Figure 3 shows the percent area under each peak, with the different sorbitan esters. These areas represent the relative abundance of the different THF types, e.g., crystalline vs. glassy. Dissimilar to observations with water, in mixtures of THF and sorbitan esters the peak at ≈1,050 cm^{-1} (glassy THF) is less prominent than the peak at the peak at 1,070 cm^{-1} (crystalline or ordered THF). This result suggests that THF is more ordered upon mixing with sorbitan esters compared to water, thereby leading to a more crystalline-like structure. THF ordering depends on the length and number of the sorbitan esters tails. THF is least ordered with Span 20, with the highest HLB number and the greatest 1,050–1,070 cm^{-1} ratio. Ordering increases when increasing the length of a single saturated tail from eleven carbons (for Span 20) to seventeen

carbons (for Span 60), as seen in Figure 2A. Also, THF is less ordered with Span 80 (one unsaturated tail with 17 carbons) than with Span 85 (three unsaturated tails with 17 carbons), as seen in Figure 2B. While Span 65 was not analyzed in detail and is not shown in Figures 2, 3, its effect on the COC band is qualitatively similar to Span 85, as it also has a low HLB number (Supplementary Figure S1.5). Analyzing in detail the effect of Span 65 on the COC band of THF will be the objective of future research.

Moreover, in pure THF, we observe a peak at 905 cm^{-1}, which corresponds to δ(C-C-O) (Harthcock, 1989) (Figure 4). Mixing THF with water causes splitting of this peak, in agreement with previous studies (Figure 4). For example, in a Raman study, the authors observed peaks at 914 cm^{-1} and 2,870–2,960 cm^{-1}, which are assigned to a ring breathing mode (Li et al., 2016). The authors report that in a 19.1 wt % THF solution, the bands centered at 914 cm^{-1} for pure THF split into two peaks at 892 and 918 cm^{-1}, due to interactions between THF and water molecules (Li et al., 2016). Another Raman study also reports a split of the peak at 916 cm^{-1} into two peaks at 920 and 891 cm^{-1} in aqueous mixtures of THF (Prasad et al., 2007). Note that the position of the peaks in Raman is shifted compared to IR. By correlating the δ(C-C-O) band to the COC stretch, we propose that the peak at approximately 890 cm^{-1} corresponds to glassy THF and the peak at 910 cm^{-1} corresponds to crystalline THF.

The δ(C-C-O) band of THF is also affected by mixing THF with sorbitan esters (cf. Figure 4). In this case, the peak at 890 cm^{-1} (glassy THF) appears as a shoulder while the dominant peak is at 910 cm^{-1} (crystalline THF), in contrast with THF-water mixtures. This effect is most marked with the most hydrophobic sorbitan esters, Span 65 and Span 85, as qualitatively seen in Figure 4. We also quantitatively analyze the overall position of the δ(C-C-O) peak, rather than the two peaks convolved under it (Figure 5). Figure 5 shows that the shift of the peak to higher wavenumbers is greatest with the most hydrophobic sorbitan ester (e.g., Span 85), in line with the greater ordering of THF, whereas the shift is smallest with the most hydrophilic sorbitan ester (Span 20). Note that while we have not analyzed Span 65 in detail, its effect on the δ(C-C-O) is qualitatively similar to Span 85 (Figure 5), with a similar HLB number. In summary, the analysis of the δ(C-C-O) confirms the hypothesis that THF interacts with sorbitan esters through H bonds. It also indicates that THF is more ordered upon mixing with sorbitan esters than with water, in agreement with the analysis of the COC stretch band of THF.

So far, we have discussed H bonding between sorbitan esters and THF. We also highlighted that THF ordering upon mixing with sorbitan esters is correlated to their HLB numbers. Now, we compare the interactions between the different sorbitan ester tails and THF. Recall that sorbitan esters with saturated tails flocculate at low THF percentages, whereas this does not occur when tails are unsaturated. This result suggests that the characteristics of the tails influence THF-sorbitan ester interactions. To probe this aspect, we examine the CH band in the spectrum of sorbitan esters (Figure 6). In our previous study, we analyzed the CH bands of THF, to study THF interactions with water (Bartokova et al., 2023b). We found that this band shifts to higher wavenumbers upon mixing THF with water (Bartokova et al., 2023b), in agreement with a study conducted by Mizuno et al. (2003). Mizuno et al. proposed that water formed a bifunctionally hydrogen-bonded hydration complex with

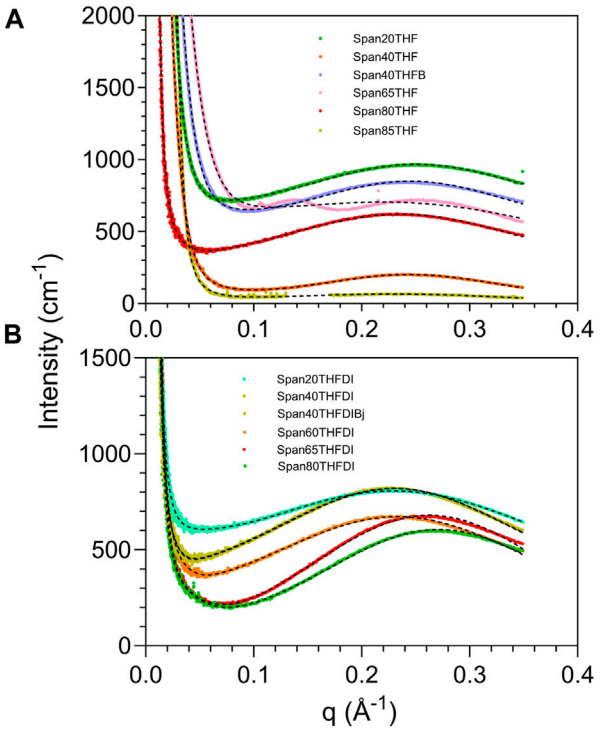

FIGURE 7
XRD patterns in the SAXS region for different sorbitan esters in either THF **(A)** or THF-DI water mixtures **(B)** containing 98% THF (v/v, relative to water). In **(A)**, Span40 THF and Span40 THF B represent replicate experiments. Similarly, in **(B)**, Span40 THF DI and Span40 THF DI Bj represent replicate experiments. These replicates are shown to allow the readers to compare replicate experiments. The comparison of the XRD of Span 85 in THF vs. THF and DI water is shown separately in Figure 8.

1,4 dioxane. In this complex, water acts both as a proton donor (in a conventional OH. . .O hydrogen bond with the ether oxygen) and as a proton acceptor (which accepts the H from the CH group, to form CH. . .OH_2) (Mizuno et al., 2003). Here, we analyze the $\nu_{as}(CH_2)$ band of sorbitan esters, to examine their interactions with THF. The second derivative of spectra allows for the identification of convoluted peaks under a band envelope in the form of negative peaks. From the second derivative, we can be confident that the THF band does not interfere with the $\nu_{as}(CH_2)$ band of sorbitan esters (Supplementary Figure S1.6). This is different from the $\nu_{s}(CH_2)$, which is heavily overlapped with the THF band and less clear to interpret, justifying our focus on the $\nu_{as}(CH_2)$ band. Our data reveal that there is a blueshift in the $\nu_{as}(CH_2)$ band of sorbitan esters with increasing THF content (Figure 6). C-H. . .O hydrogen bonds are widely accepted, as discussed above. They manifest in IR as a shortening of the C-H bond (not lengthening like a regular H bond) and therefore a blue shift (Mizuno et al., 2003). Therefore, the data indicate that with increasing THF percentages in binary mixtures of THF and sorbitan esters, C-H. . .O bonding becomes stronger, as expected. Importantly, the effect of this interaction is most significant in Span 40 and 60. Recall that Span 40 and Span 60 form flocs at low THF percentages relative to water, whereas Span 20, Span 80 and Span 85 form emulsions (cf. Supplementary Figure S1.2). This observation, in conjunction with the analysis of the CH

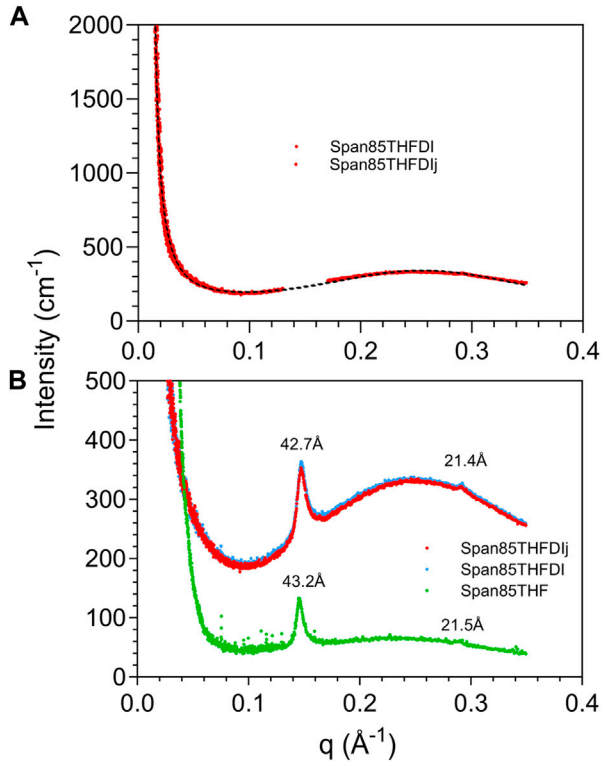

FIGURE 8
XRD patterns in the SAXS region for Span 85 in either pure THF or THF and DI water. In the figure legend, Span85THFDI and Span85THFDIJ represent replicate experiments, shown to highlight the reproducibility of the data. In **(A)** the peak at 42.7 Å has been removed for the purpose of the fit, while in **(B)** the peak is shown.

band, indicates that Span 40 and Span 60 interact with THF more strongly than Span 20, Span 80 and Span 85. In contrast, Span 40 and Span 60 interact with water less strongly than Span 20, Span 80 and Span 85. Both the length and the saturation of the tail play a role. Span 40 and Span 60 have saturated tails, whereas Span 80 and Span 85 have unsaturated tails. Span 20 also has a saturated tail, but the tail is short. In light of these results, we propose that separation between THF and water occurs *primarily* (but not exclusively) because the hydrophilic head of Span 20, Span 80 and Span 85 competes for interactions with water against THF. This is in line with our previous study, where proposed that Span 80 competes against THF for interactions with water, based on the analysis of the OH stretch band (Bartokova et al., 2023b). In contrast, we propose that separation between THF and water occurs *primarily* (but not exclusively) due to preferential interactions between the tail of Span 40 and Span 60 and THF. Note that we are not excluding interactions between THF and the tails of Span 20, Span 80 and Span 85, or between water and the heads of Span 40 and Span 60. Indeed, SAXS data demonstrate interactions between the heads of all sorbitan esters and water, as discussed below.

In particular, we use SAXS to compare the self-assembly of sorbitan esters in pure THF and with low (2%) water percentages relative to THF. While higher water percentages lead to emulsification of larger droplets or bulk separation, at low water percentages we can observe the onset of THF-water separation. In pure THF, we propose that sorbitan esters can interact with the solvent through either their heads or tails, leading to their self-assembly into micelles with their heads pointing outwards or inwards. This hypothesis is confirmed by SAXS data (Figures 7, 8). The SAXS patterns of all sorbitan esters in pure THF display broad peaks, which are characteristic of micelles with their heads pointing outwards or inwards (Bartokova et al., 2023a). In THF, either the heads or the tails of the sorbitan esters could be pointing outwards, because both have the ability to interact with THF. This is similar to observations of stearic acid in THF, as reported in our previous study (Bartokova et al., 2023a). Span 85 also displays a crystalline peak, which indicates that it is not fully solubilized in THF. In pure THF, the self-assembled structures formed by Span 40 and Span 65 are mass fractals, whereas surface fractals are observed for Span 20, Span 80 and Span 85, as summarized in Table 3 (results are less clear for Span 60). These results correlate to the liquid vs. solid state of neat sorbitan esters. Neat Span 40 and Span 65 are solids, whereas Span 20, Span 80 and Span 85 are liquids at 20°C, at which measurements were conducted. Optical microscopy observations show self-assembly into large flocs with Span 40, Span 60 and Span 65 in pure THF (Supplementary Figure S1.7). While the scales observed with optical microscopy and SAXS are clearly different, we are comparing these two techniques because fractals are scale invariant. In THF, the persistence length determined based on the peak center and from the standard deviation of the zero mean Gaussian peak are ≈25 Å for Span 20 and Span 40 and larger (≈27 Å) for Span 80, Span 65 and Span 85, consistent with their larger size. We interpret these values as the distance between the centers of micelles with their heads pointing outwards or inwards. Interestingly, in THF, we also identify a significantly smaller, second persistence length (≈16 Å for Span 20, Span 40, Span 80 and Span 65, and ≈ 21 Å for Span 85), based on the standard deviation of the non-zero mean Gaussian peak. We ascribe the difference between these two persistence lengths to the limited order in mixtures of sorbitan esters in THF. With 2% water in THF, self-assembled structures of sorbitan esters are surface fractals in all cases, except Span 85. Span 85 is a mass fractal and displays a crystalline peak in its SAXS pattern, similar to observations in pure THF. This result could be due to incomplete hydration of Span 85 during the time frame analyzed, with the small amounts of water added. We ascribe the transition from mass to surface fractals for all other sorbitan esters to the fact that water promotes the formation of micelles with their heads pointing inwards. These contain water in their interior, towards which the heads point. Note that while SAXS patterns could indicate either micelles with heads pointing outwards or inwards, samples contained 2% water and 98% THF. In such samples, THF should be the continuous phase because of its high percentage, while water should be inside the micelle. Since the hydrophobic Span tails cannot interact with water, the hydrophilic head would be pointing inwards. Dissimilar to observations with 2% water, in THF, either the heads or the tails of the sorbitan esters could be pointing outwards. This is because both have the ability to interact with THF, as mentioned above. As a result of the enhanced ordering induced by addition of 2% water, we find a single persistence length. Specifically, with 2% water, the average persistence length determined for the different sorbitan esters based on the peak center and from the standard deviation of

the zero mean Gaussian peak is ≈25 Å. This value is close to the persistence length determined based on the standard deviation of the nonzero mean Gaussian peak. Once again, this is in contrast with THF, where we have less ordered self-assembled structures and identified two persistence lengths. Note that we did not conduct SAXS experiments with high water percentages. In this case, we would expect that sorbitan esters would be forming micelles, which would contain THF in their interior and would have their hydrophilic heads pointing outwards towards the water.

In summary, IR data suggest that the longer, saturated tail of some sorbitan esters (e.g., Span 40 and Span 60) interact with THF more strongly than the shorter, saturated tail of Span 20, or the unsaturated tails of Span 80 and Span 85. SAXS data complement these findings. They show that interactions between all sorbitan esters and water play a role in THF-water separation, beyond differences in the way they interact with THF. Indeed, in all cases 2% water enhances ordering, since it favors the formation of micelles with water in their interior.

4 Conclusion

Bottle tests, optical microscopy and FTIR spectromicroscopy show that sorbitan esters (Span 20, Span 40, Span 60, Span 80, Span 65 and Span 85) separate THF and water, which would otherwise be miscible due to H bonding. Separation occurs with up to 70% THF (v/v, relative to water), at THF to water ratios dependent on the sorbitan ester structure. Span 80 and Span 85 have double bonds in their tails. Double bonds in the tail (i.e., unsaturated tails) promote separation at the lowest THF percentages. In contrast, Span 40 and Span 60 (with saturated tails) flocculate at the lowest THF percentages (10%–30% THF) and do not effectively separate these THF-water mixtures. This suggests weaker interactions with water, and hence lower solubility at high water percentages. Saturated, but shorter tails (e.g., Span 20) still allow separation at low THF percentages.

We use ATR-FTIR to study separation mechanisms between THF and water by sorbitan esters. ATR-FTIR reveals that mixing with water disorders THF, resulting in an increase of the percentage of glassy to crystalline THF.

Sorbitan esters impede THF-water interactions. Similar to water, they H bond with THF. However, dissimilar to water, they order THF. Ordering increases with tail length (e.g., from Span 20 to Span 60) and with increasing number of tails (e.g., from Span 80 to Span 85). This is reflected in the COC and δ(C-C-O) band of THF.

Furthermore, we observe a blueshift in the $\nu_{as}(CH_2)$ band of sorbitan esters upon mixing with increasing THF percentages, because of the formation of C-H. . .O H bonds. The blueshift is most marked for Span 40 and 60. This result indicates that Span 40 and Span 60 interact with THF more strongly than Span 20, Span 80 and Span 85. In contrast, Span 40 and Span 60 interact with water less strongly than Span 20, Span 80 and Span 85, as indicated by their flocculation at the lowest THF percentages (10%–30% THF, v/v relative to water).

Based on these results, we propose that separation between THF and water occurs due to two primary mechanisms, depending on the sorbitan ester characteristics. Specifically, separation occurs *primarily* (but not exclusively) because the hydrophilic head of Span 20, Span 80 and Span 85 compete for interactions with water against THF. In contrast, separation occurs *primarily* (but not exclusively) due to preferential interactions between the tail of Span 40 and Span 60 and THF. Note that we are not contending that these are the only mechanisms involved. Indeed, THF interacts with the tails of all sorbitan esters, and water interacts with their heads.

The role of water-sorbitan ester interactions on THF-water separation is highlighted by SAXS data. In THF, sorbitan esters self-assemble into micelles with their heads pointing outwards or inwards, because both the heads and the tails of sorbitan esters interact with THF. Both types of micelles further assemble to form either closed-packed clusters (surface fractals, in the case of Span 20, Span 80, and Span 85), or open-packed clusters (mass fractals, in the case of Span 40, Span 60 and Span 65). In THF, we identify two different persistence lengths, because of the limited order of sorbitan ester self-assembled structures. With 2% water, we observe a transition from mass to surface fractals in all cases except Span 85, possibly due to its incomplete hydration. Under these conditions, sorbitan esters self assemble into micelles with their heads pointing inwards, which host water in their interior. We identify a single persistence length (≈25 Å), which corresponds to the distance between the micelle centers. This shows enhanced ordering.

Our future research will focus on further elucidating how separation mechanisms are affected by the tail structure, for different amphiphiles, including ones the head of which does not interact with THF, as well as others with varying heads that H bond THF. This research is part of our overall goal of developing a predictive toolbox to optimize solvent separation from water.

Data availability statement

The original contributions presented in the study are included in the article/Supplementary Material, further inquiries can be directed to the corresponding author.

Author contributions

BB: Data curation, Formal Analysis, Investigation, Validation, Visualization, Writing–original draft, Writing–review and editing. AM: Data curation, Formal Analysis, Investigation, Methodology, Software, Validation, Visualization, Writing–original draft, Writing–review and editing. TL: Data curation, Formal Analysis, Software, Visualization, Writing–review and editing. EP: Conceptualization, Data curation, Formal Analysis, Funding acquisition, Investigation, Project administration, Resources, Software, Supervision, Validation, Visualization, Writing–original draft, Writing–review and editing.

Funding

The author(s) declare financial support was received for the research, authorship, and/or publication of this article. Part of the research described in this paper was performed at the Canadian Light Source, a national research facility of the University of

Saskatchewan, which is supported by the Canada Foundation for Innovation (CFI), the Natural Sciences and Engineering Research Council (NSERC), the National Research Council (NRC), the Canadian Institutes of Health Research (CIHR), the Government of Saskatchewan, and the University of Saskatchewan. The authors acknowledge the support of the Natural Sciences and Engineering Research Council of Canada (provided through an NSERC Discovery grant, awarded to EP, PIN 537871).

Conflict of interest

The authors declare that the research was conducted in the absence of any commercial or financial relationships that could be construed as a potential conflict of interest.

Publisher's note

Supplementary material

The Supplementary Material for this article can be found online at: https://www.frontiersin.org/articles/10.3389/frsfm.2023.1329058/full#supplementary-material

References

Aliaga, C., Tsung, C. K., Alayoglu, S., Komvopoulos, K., Yang, P., and Somorjai, G. A. (2011). Sum frequency generation vibrational spectroscopy and kinetic study of 2-methylfuran and 2, 5-dimethylfuran hydrogenation over 7 nm platinum cubic nanoparticles. *J. Phys. Chem. C* 115, 8104–8109. doi:10.1021/jp111343j

Barman, S. R., Banerjee, P., Mukhopadhayay, A., and Das, P. (2017). Biodegradation of acenapthene and naphthalene by Pseudomonas mendocina: process optimization, and toxicity evaluation. *J. Environ. Chem. Eng.* 5, 4803–4812. doi:10.1016/j.jece.2017.09.012

Bartokova, B., Laredo, T., Marangoni, A. G., and Pensini, E. (2023a). Mechanism of tetrahydrofuran separation from water by stearic acid. *J. Mol. Liq.* 391, 123262. doi:10.1016/j.molliq.2023.123262

Bartokova, B., Marangoni, A. G., Laredo, T., and Pensini, E. (2023b). Role of hydrogen bonding on solvent separation using amphiphilic sorbitan ester. Colloids and Surfaces C. 1, 100004.

Bartokova, B., Marangoni, A. G., Laredo, T., Stobbs, J., Meszaros, P., and Pensini, E. (2023c). Effect of hydrogen bonding on the mixing behaviour of ternary aqueous mixtures. *J. Mol. Liq.* 283, 122124. doi:10.1016/j.molliq.2023.122124

Belhaj, A., Desnoues, N., and Elmerich, C. (2002). Alkane biodegradation in *Pseudomonas aeruginosa* strains isolated from a polluted zone: identification of alkB and alkB-related genes. *Res. Microbiol.* 153, 339–344. doi:10.1016/s0923-2508(02)01333-5

Besha, A. T., Bekele, D. N., Naidu, R., and Chadalavada, S. (2018). Recent advances in surfactant-enhanced In-Situ Chemical Oxidation for the remediation of non-aqueous phase liquid contaminated soils and aquifers. *Environ. Technol. Innovation* 9, 303–322. doi:10.1016/j.eti.2017.08.004

Boonchan, S., Britz, M. L., and Stanley, G. A. (1998). Surfactant-enhanced biodegradation of high molecular weight polycyclic aromatic hydrocarbons by Stenotrophomonas maltophilia. *Biotechnol. Bioeng.* 59, 482–494. doi:10.1002/(sici)1097-0290(19980820)59:4<482::aid-bit11>3.0.co;2-c

de Brito Cardoso, G., Nascimento Souza, I., Mourão, T., Freire, M. G., Soares, C. M. F., and Silva Lima, Á. (2014). Novel aqueous two-phase systems composed of acetonitrile and polyols: phase diagrams and extractive performance. *Sep. Purif. Technol.* 124, 54–60. doi:10.1016/j.seppur.2014.01.004

Dhamole, P. B., Mahajan, P., and Feng, H. (2010). Phase separation conditions for sugaring-out in Acetonitrile–Water systems. *J. Chem. Eng. Data* 55 (9), 3803–3806. doi:10.1021/je1003115

Earnden, L., Marangoni, A. G., Laredo, T., Stobbs, J., Marshall, T., and Pensini, E. (2022a). Decontamination of water co-polluted by copper, toluene and tetrahydrofuran using lauric acid. *Sci. Rep.* 12, 15832–15920. doi:10.1038/s41598-022-20241-4

Earnden, L., Marangoni, A. G., Laredo, T., Stobbs, J., and Pensini, E. (2022b). Mechanisms of separation between tetrahydrofuran and water using hydroxystearic acid. *Phys. Fluids* 34, 097119. doi:10.1063/5.0108008

Earnden, L., Marangoni, A. G., Laredo, T., Stobbs, J., and Pensini, E. (2022c). Self-Assembled glycerol monooleate demixes miscible liquids through selective hydrogen bonding to water. *J. Mol. Liq.* 367, 120551. doi:10.1016/j.molliq.2022.120551

Fleyfel, F., and Devlin, J. P. (1991). Carbon dioxide clathrate hydrate epitaxial growth: spectroscopic evidence for formation of the simple type-II carbon dioxide hydrate. *J. Phys. Chem.* 95, 3811–3815. doi:10.1021/j100162a068

Hall, J., Soole, K., and Bentham, R. (2011). Hydrocarbon phytoremediation in the family Fabacea—a review. *Int. J. phytoremediation* 13, 317–332. doi:10.1080/15226514.2010.495143

Harthcock, M. A. (1989). Probing the complex hydrogen bonding structure of urethane block copolymers and various acid containing copolymers using infra-red spectroscopy. *Polymer* 30, 1234–1242. doi:10.1016/0032-3861(89)90041-4

Hu, D., Li, X., Chen, Z., Cui, Y., Gu, F., Jia, F., et al. (2018). Performance and extracellular polymers substance analysis of a pilot scale anaerobic membrane bioreactor for treating tetrahydrofuran pharmaceutical wastewater at different HRTs. *J. Hazard. Mater.* 342, 383–391. doi:10.1016/j.jhazmat.2017.08.028

Isaacson, C., Mohr, T. K., and Field, J. A. (2006). Quantitative determination of 1, 4-dioxane and tetrahydrofuran in groundwater by solid phase extraction GC/MS/MS. *Environ. Sci. Technol.* 40, 7305–7311. doi:10.1021/es0615270

Jessop, P., and Cunningham, M. (20206). *CO2-switchable materials*. London, United Kingdom: Royal Society of Chemistry.

Kolehmainen, E., and Turunen, I. (2007). Micro-scale liquid–liquid separation in a plate-type coalescer. *Chem. Eng. Process. Process Intensif.* 46, 834–839. doi:10.1016/j.cep.2007.05.027

Lee, J., Cho, J., Kim, D. M., and Park, S. (2011). Separation of tetrahydrofuran and water using pressure swing distillation: modeling and optimization. *Korean J. Chem. Eng.* 28, 591–596. doi:10.1007/s11814-010-0467-1

Leontowich, A. F., Gomez, A., Diaz Moreno, B., Muir, D., Spasyuk, D., King, G., et al. (2021). The lower energy diffraction and scattering side-bounce beamline for materials science at the Canadian Light Source. *J. Synchrotron Radiat.* 28, 961–969. doi:10.1107/s1600577521002496

Levenberg, K. (1944). A method for the solution of certain non-linear problems in least squares. *Q. Appl. Math.* 2, 164–168. doi:10.1090/qam/10666

Li, H., Stanwix, P., Aman, Z., Johns, M., May, E., and Wang, L. (2016). Raman spectroscopic studies of clathrate hydrate formation in the presence of hydrophobized particles. *J. Phys. Chem. A* 120, 417–424. doi:10.1021/acs.jpca.5b11247

Liu, L., Xia, Y., Wang, L., Shi, R., Yan, S., Zhao, X., et al. (2022). Cyanate ester resin with high heat-resistance and degradable diacetal structure: synthesis, polymerization, and properties. *Macromol. Mater. Eng.* 307, 2200423. doi:10.1002/mame.202200423

Longeras, O., Gautier, A., Ballerat-Busserolles, K., and Andanson, J. M. (2020). Deep eutectic solvent with thermo-switchable hydrophobicity. *ACS Sustain. Chem. Eng.* 8, 12516–12520. doi:10.1021/acssuschemeng.0c03478

Malakahmad, A., and Ho, L. L. H. (2017). UV/H2O2 oxidation process optimization by response surface methodology for removal of polycyclic aromatic hydrocarbons (PAHs) from water. *Desalination Water Treat.* 65, 408–417. doi:10.5004/dwt.2017.20278

Mammone, J. F., Sharma, S. K., and Nicol, M. (1980). Raman spectra of methanol and ethanol at pressures up to 100 kbar. *J. Phys. Chem.* 84, 3130–3134. doi:10.1021/j100460a032

Marquardt, D. W. (1963). An algorithm for least-squares estimation of nonlinear parameters. *J. Soc. Industrial Appl. Math.* 11, 431–441. doi:10.1137/0111030

Marshall, T., Earnden, L., Marangoni, A. G., Laredo, T., and Pensini, E. (2022). Cubic mesophases of self-assembled amphiphiles separate miscible solvents. *Colloids Surfaces A* 650, 129548. doi:10.1016/j.colsurfa.2022.129548

Mizuno, K., Imafuji, S., Fujiwara, T., Ohta, T., and Tamiya, Y. (2003). Hydration of the CH groups in 1,4-dioxane probed by NMR and IR: contribution of blue-shifting CH···OH 2 hydrogen bonds. *J. Phys. Chem. B* 107, 3972–3978. doi:10.1021/jp021712+

Patel, V., Marangoni, A. G., Mirzaee Ghazani, S., Laredo, T., Stobbs, J., and Pensini, P. (2023). Effect of bacterial surfactants on the phase behavior of miscible pollutants in water. *Colloids Surf. C* 1, 100013. doi:10.1016/j.colsuc.2023.100013

Prasad, P. S. R., Prasad, K. S., and Thakur, N. K. (2007). Laser Raman spectroscopy of THF clathrate hydrate in the temperature range 90–300 K. *Spectrochim. Acta Part A* 68, 1096–1100. doi:10.1016/j.saa.2007.06.049

Sales, C. M., Grostern, A., Parales, J. V., Parales, R. E., and Alvarez-Cohen, L. (2013). Oxidation of the cyclic ethers 1, 4-dioxane and tetrahydrofuran by a monooxygenase in two Pseudonocardia species. *Appl. Environ. Microbiol.* 79, 7702–7708. doi:10.1128/aem.02418-13

Sionkowska, A., and Płanecka, A. (2013). Preparation and characterization of silk fibroin/chitosan composite sponges for tissue engineering. *J. Mol. Liq.* 178, 5–14. doi:10.1016/j.molliq.2012.10.042

Souza, R. L., Lima, R. A., Coutinho, J. A., Soares, C. M., and Lima, Á. S. (2015). Aqueous two-phase systems based on cholinium salts and tetrahydrofuran and their use for lipase purification. *Sep. Purif. Technol.* 155, 118–126. doi:10.1016/j.seppur.2015.05.021

Sun, Y., Zhou, Q., Xu, Y., Wang, L., and Liang, X. (2011). Phytoremediation for co-contaminated soils of benzo [a] pyrene (B [a] P) and heavy metals using ornamental plant Tagetes patula. *J. Hazard. Mater.* 186, 2075–2082. doi:10.1016/j.jhazmat.2010.12.116

Tabata, M., Kumamoto, M., and Nishimoto, J. (1994). Chemical properties of water-miscible solvents separated by salting-out and their application to solvent extraction. *Anal. Sci.* 10, 383–388. doi:10.2116/analsci.10.383

Toby, B. H., and Von Dreele, R. B. (2013). GSAS-II: the genesis of a modern open-source all purpose crystallography software package. *J. Appl. Crystallogr.* 46, 544–549. doi:10.1107/s0021889813003531

Urtiaga, A., Gómez, P., Arruti, A., and Ortiz, I. (2014). Electrochemical removal of tetrahydrofuran from industrial wastewaters: anode selection and process scale-up. *J. Chem. Technol. Biotechnol.* 89, 1243–1250. doi:10.1002/jctb.4384

Von Dreele, R. B. (2014). Small-angle scattering data analysis in GSAS-II. *J. Appl. Crystallogr.* 47, 1784–1789. doi:10.1107/s1600576714018366

Wang, B., Ezejias, T., Feng, H., and Blaschek, H. (2008). Sugaring-out: a novel phase separation and extraction system. *Chem. Eng. Sci.* 63, 2595–2600. doi:10.1016/j.ces.2008.02.004

Wang, W. H., Hoag, G. E., Collins, J. B., and Naidu, R. (2013). Evaluation of surfactant-enhanced *in situ* chemical oxidation (S-isco) in contaminated soil. *Soil Pollut.* 224, 1713. doi:10.1007/s11270-013-1713-z

Yin, Y., Yang, Y., de Lourdes Mendoza, M., Zhai, S., Feng, W., Wang, Y., et al. (2017). Progressive freezing and suspension crystallization methods for tetrahydrofuran recovery from Grignard reagent wastewater. *J. Clean. Prod.* 144, 180–186. doi:10.1016/j.jclepro.2017.01.012

Yoshikawa, M., Masaki, K., and Ishikawa, M. (2002). Pervaporation separation of aqueous organic mixtures through agarose membranes. *J. Membr. Sci.* 205, 293–300. doi:10.1016/s0376-7388(02)00131-x